catalysts

MDPI

Article

Description of Transport Tunnel in Haloalkane Dehalogenase Variant LinB D147C+L177C from *Sphingobium japonicum*

Iuliia Iermak [1], Oksana Degtjarik [2], Petra Havlickova [3], Michal Kuty [3], Radka Chaloupkova [4], Jiri Damborsky [4,5], Tatyana Prudnikova [3,*] and Ivana Kuta Smatanova [3,*]

1 Department of Structural Cell Biology, Max Planck Institute of Biochemistry, Am Klopferspitz 18, 82152 Martinsried, Germany; iermak@biochem.mpg.de
2 Department of Structural Biology, Weizmann Institute of Science, Rehovot 7610001, Israel; degtjarik648@gmail.com
3 Faculty of Science, University of South Bohemia in Ceske Budejovice, Branisovska 1760, 37005 Ceske Budejovice, Czech Republic; havlickova.pet@seznam.cz (P.H.); kutym@seznam.cz (M.K.)
4 Loschmidt Laboratories, Department of Experimental Biology and RECETOX, Faculty of Science, Masaryk University, Kamenice 5, 62500 Brno, Czech Republic; radka@chemi.muni.cz (R.C.); 1441@mail.muni.cz (J.D.)
5 International Clinical Research Center, St. Anne's University Hospital Brno, Pekarska 53, 65691 Brno, Czech Republic
* Correspondence: talianensis@gmail.com (T.P.); ivanaks@seznam.cz (I.K.S.)

Abstract: The activity of enzymes with active sites buried inside their protein core highly depends on the efficient transport of substrates and products between the active site and the bulk solvent. The engineering of access tunnels in order to increase or decrease catalytic activity and specificity in a rational way is a challenging task. Here, we describe a combined experimental and computational approach to characterize the structural basis of altered activity in the haloalkane dehalogenase LinB D147C+L177C variant. While the overall protein fold is similar to the wild type enzyme and the other LinB variants, the access tunnels have been altered by introduced cysteines that were expected to form a disulfide bond. Surprisingly, the mutations have allowed several conformations of the amino acid chain in their vicinity, interfering with the structural analysis of the mutant by X-ray crystallography. The duration required for the growing of protein crystals changed from days to 1.5 years by introducing the substitutions. The haloalkane dehalogenase LinB D147C+L177C variant crystal structure was solved to 1.15 Å resolution, characterized and deposited to Protein Data Bank under PDB ID 6s06.

Keywords: bacterial enzyme; haloalkane dehalogenase; mutant form; crystallization; tertiary structure; disulfide bond; protein engineering; molecular dynamics; access tunnel; substrate specificity

Citation: Iermak, I.; Degtjarik, O.; Havlickova, P.; Kuty, M.; Chaloupkova, R.; Damborsky, J.; Prudnikova, T.; Kuta Smatanova, I. Description of Transport Tunnel in Haloalkane Dehalogenase Variant LinB D147C+L177C from *Sphingobium japonicum*. *Catalysts* **2021**, *11*, 5. https://dx.doi.org/10.3390/catal11010005

Received: 20 November 2020
Accepted: 18 December 2020
Published: 23 December 2020

1. Introduction

The members of the haloalkane dehalogenase family (EC 3.8.1.5) are responsible for the cleavage of the carbon–halogen bond in various halogenated compounds, one of the key reactions in the aerobic degradation of halogenated environmental pollutants [1]. Haloalkane dehalogenase LinB from a bacterium *Sphingobium japonicum* UT26 is able to convert cyclic dienes, broad range of halogenated alkanes and alkenes to their corresponding alcohols and halide ions, which comprise a large group of environmental pollutants [2]. Due to its broad substrate specificity, LinB has a potential for applications in biosensing and biodegradation of environmental pollutants [3].

The catalytic cycle of LinB is similar to all haloalkane dehalogenases (HLDs) and was described earlier [4]. The cleavage of the carbon–halogen bond is the fastest step in catalytic cycle, while the hydrolysis of the alkyl-enzyme intermediate is rate-limiting step

in the kinetic mechanism [4]. The cap domain is flexible, allowing for the fast exchange of products and substrates between the active site and the bulk solvent [4].

Structure of LinB is typical for α/β-hydrolase proteins. It consists of conserved α/β core domain and upper α-helical cap domain, which is sequentially and structurally varied among dehalogenases [5]. The core domain (residues 3–132, 214–296) consists of a central twisted eight-stranded β-pleated sheet, flanked by two on one side and four on the other side α-helices. The cap domain (residues 133–213) is formed by five α-helices (Figure 1).

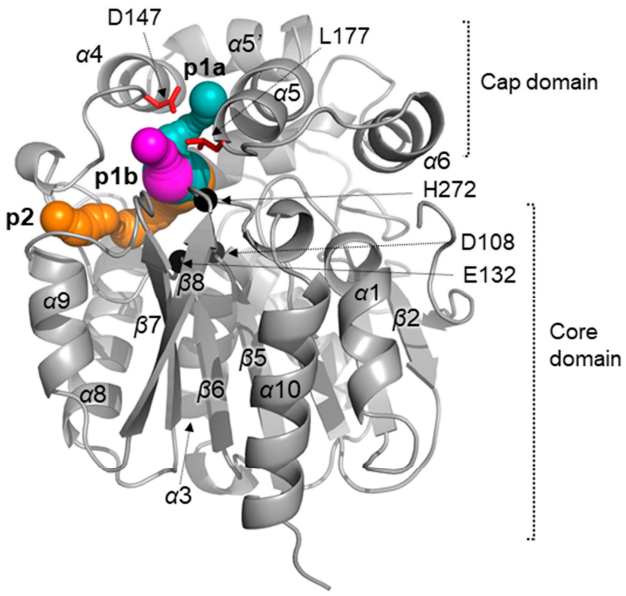

Figure 1. Overall structure of the wild type LinB dehalogenase (PDB ID 1cv2, [5]). The upper, lower tunnels and slot are shown as magenta, cyan and orange spheres, respectively. The catalytic triad residues (Asp108, Glu132 and His272) are shown as black spheres. The studied mutations are shown as red sticks.

LinB belongs to the HLD-II subfamily [6]. The catalytic nucleophile Asp108 is situated at the "nucleophile elbow" between β5 strand and α3 helix, base His272 is located in β8-α11 loop and catalytic acid lies after strand β6. Halide stabilizing residues Asn38 and Trp109 are located on the loops between β3-α1 and β5-α3, respectively [5,7]. The active site cavity of the enzyme is one of the largest among structurally characterized dehalogenases (276 A^3). Due to the large active site cavity LinB prefers to utilize long-chain and bulky substrates [8]. The deeply buried cavity of the enzyme is connected with surrounding solvent by tunnels identified by the Caver program [9] (Figure 1): p1 (main tunnel) and p2 (slot, [10]). The main tunnel branches into two tunnels with one asymmetric opening: p1a or upper tunnel (residues Gln146, Asp147, Gly176 and Leu177) and p1b or lower tunnel (Gln146, Leu177, Ala247, Ala271 and His272) [10,11].

Architecture, chemical properties and dynamics of the access tunnels significantly affect enzyme catalysis since they have a major influence on exchange rates of substrates and products [10–14]. In addition, tunnels may also affect other enzyme properties, such as substrate specificity and timing stages of the reactions [15,16]. Therefore, several variants of LinB have been designed to explore structure-function relationships of the enzyme and optimize its properties for biotechnological applications [12]. It has been experimentally demonstrated that substitution of Leu177 located in the mouth of the main tunnel can modify the activity and specificity of LinB enzyme [17]. LinB L177W variant with Leu177 replaced by bulky Trp shows a dramatic decrease in the activity of the enzyme towards the best substrate 1,2-dibromoethane [17]. Moreover, the kinetic analysis shows that the introduction of the Trp at the tunnel opening changes the mechanism of bromide release from a one-step process in the wild type to a two-step mechanism in L177W mutant [17]. In contrast, LinB W140A+F143L+L177W+I211L variant, in which the main

tunnel is significantly narrowed by the same substitution L177W, but the introduced alternative access pathway is opened, shows a dramatic improvement of the enzymatic catalysis [12]. As was shown by molecular dynamics simulations, the de novo created tunnel is used for transport of the catalysis products and water molecules, which are a co-substrate for the reaction [12].

In this study, we have focused on LinB D147C+L177C, in which mutations were designed to block the main tunnel by formation of a new disulfide bridge inside of the main tunnel. This mutant with decreased catalytic rate was intended to serve as a negative control and a template for a new tunnel creation for the biochemical characterization [12].

Here we present the analysis of the overall fold, access tunnels, and docked protein-substrate complexes in the newly reported crystal structure of LinB D147C+L177C mutant (PDB ID: 6s06, this study) and molecular dynamics (MD) model LinB^{MD} D147C+L177C. The tunnels were compared with previously reported crystal structures of LinB WT (PDB ID: 2bfn, [18]), LinB L177W (PDB ID: 4ibq, [19]) and LinB W140A+F143L+L177W+I211L (PDB ID: 5lka, [12]) mutants.

2. Results and Discussion

2.1. Crystal Structure of LinB D147C+L177C

After initial screening of the crystallization conditions of LinB D147C+L177C by application of various screens from Hampton Research (USA), Molecular Dimensions (UK), and Qiagen (The Netherlands) only amorphous precipitation was observed. Further optimization by verification of protein concentration, temperature, ratio in protein-precipitant drop, as well as additive application (Additive screen from Hampton Research) did not improve the result. Finally, one and a half year passed until the appearance of the first crystals, which were grown only in one crystallization drop in the form of rod clusters typical of LinB WT (Figure 2a). Furthermore, other similarly shaped crystals were found two and a half years after the initial screening. Any attempts to reproduce the crystals, optimize them by microseeding, or to speed up the crystallization process by adding an oxidizing (oxidized glutathione) or reducing (reduced glutathione, DTT or mercaptoethanol) agents to the crystallization cocktail were not successful. The disulfide bridge in the vicinity of the active site deep inside the structure probably provided the torsion and additional pressure that make the protein sample unstable and difficult to crystallize. We assume that the crystals grown only after disruption of the disulfide bridge between 147C and 177C in the protein sample.

The crystals of LinB D147C+L177C grew in the condition composed of 0.2 M magnesium chloride and 20% w/v PEG 3350. Crystallization in the presence of Ca^{2+} or Mg^{2+} ions is a common characteristic of LinB variants as well as other haloalkane dehalogenases [12,20–22]. Two out of three magnesium ions resolved in LinB D147C+L177C structure are involved in crystal contacts between symmetry-related molecules via their hydration shell (Figure 2b), acting as a counterion between negatively charged aspartates and glutamate.

LinB D147C+L177C crystals belong to $P2_12_12_1$ space group with one protein molecule in the asymmetric unit. Even though the diffraction data were collected to atomic resolution of 1.15 Å, which allowed detailed modelling of LinB D147C+L177C structure, the electron density for amino acids close to mutation sites, especially for amino acids 145–148, is of poor quality, indicating heterogeneity of protein conformations within the crystal (Figure 3a). In our structure, the distance between Cys147 and Cys177 is 4.6 Å (Figure 3a), which is too large for the disulfide bridge to be formed, and the main chain atoms of residues 144–150 should be shifted considerably for that. On the other hand, LinB D147C+L177C was shown to have lower activity for the majority of tested halogenated substrates compared to LinB WT [12]. Crystal contacts near Cys147 and Cys177, for example, hydrogen bonds between Gln152 and Gln165 of the symmetry-related molecule (Figure 3b), are a possible explanation for cysteine bridge disruption.

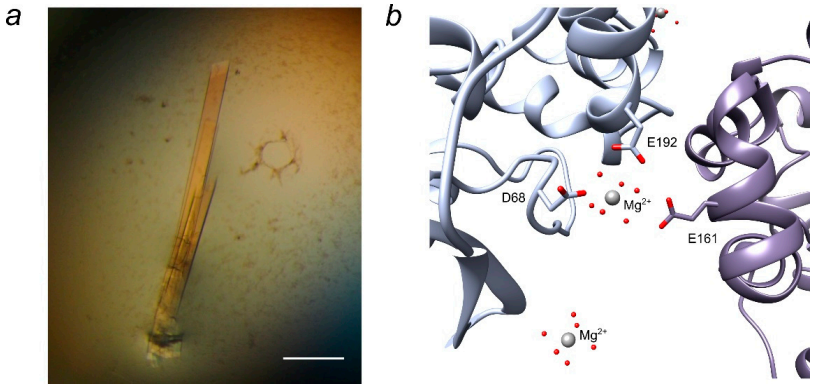

Figure 2. LinB D147C+L177C crystals and crystal contacts. (**a**) Rod-like crystals of LinB 147C+L177C from condition #53 of PEGs Suite, the scale bar is 200 µm; (**b**) Mg^{2+} ion participating in crystal contact via its hydration shell. The view is created by UCSF Chimera version 1.11.2 [23] and PyMOL Molecular Graphics System, Version 1.8 [24].

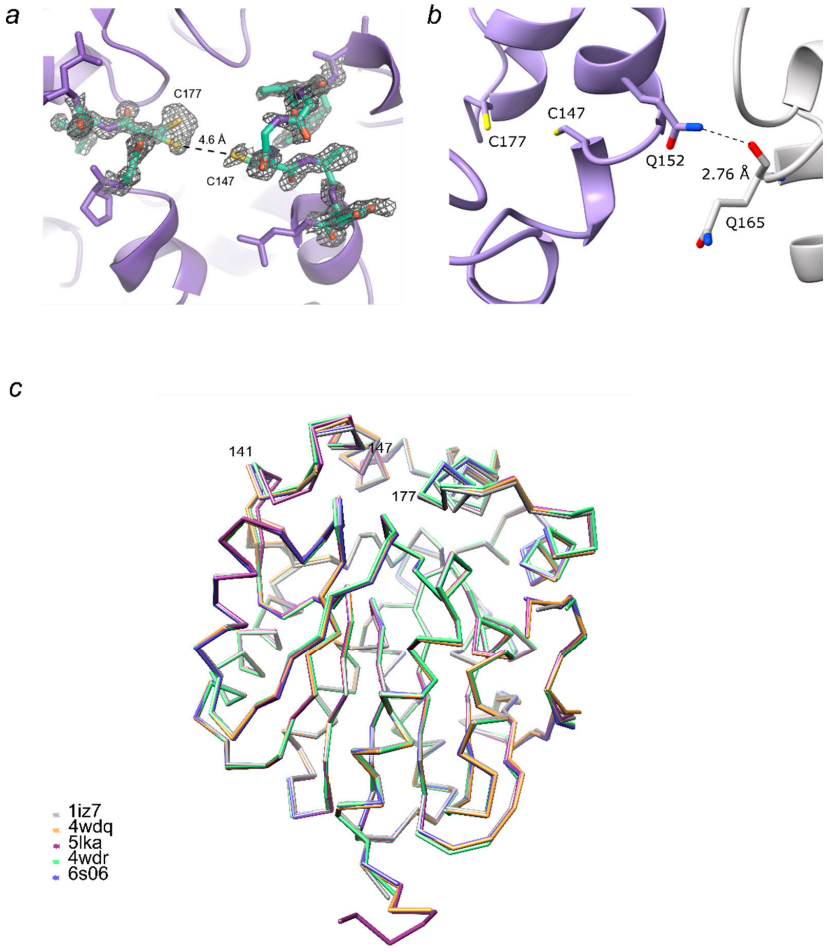

Figure 3. Structure details of LinB D147C+L177C and overlay of LinB variants. (**a**) Electron density map contoured at 1 σ for the substituted residues Cys147 and Cys177 with neighboring residues; the residues 144–150 and 176–178 are displayed as sticks and colored by the elements; (**b**) crystal contact represented by hydrogen bond between amino group of Gln152 and backbone oxygen of Gln165 of symmetry-related molecule; (**c**) LinB variants are shown as a backbone only, LinB WT (PDB ID: 1iz7, [25]) in grey; LinB L177W (PDB ID: 4wdq, [12]) in orange; LinB W140A+F143L+L177W+I211L in purple (PDB ID: 5lka, resolution 1.30 Å, chain A, [12]) and green (PDB ID: 4wdr, resolution 2.50 Å, chain A, [12]); and LinB D147C+L177C (PDB ID: 6s06, this study) in blue.

The overall fold of LinB D147C+L177C is similar to that of the wild-type LinB, with the root mean square deviation (RMSD) of only 0.30 Å for all main-chain atoms (Figure 3c). RMSD for superposition of LinB D147C+L177C with LinB L177W (PDB ID: 4wdq, [12]) is 0.23 Å; for LinB D147C+L177C with LinB W140A+F143L+L177W+I211L is 0.27 Å (PDB ID: 5lka, [5]), 0.32 Å (PDB ID: 4wdr, chain A, [12]) and 0.37 Å (PDB ID: 4wdr, chain B, [12]). Amino-acid region 141-147 showed the greatest variability among the LinB variants due to both mutations and crystal contacts. RMSD for all structures was calculated using the Superpose Molecules tool by Secondary Structure Matching [26] in the CCP4 program package [27].

2.2. Molecular Dynamics Simulations and Molecular Docking Studies with LinB D147C+L177C

Molecular dynamics simulations and molecular docking studies with LinB D147C+L177C were done to explain the mutant flexibility due to the presence of disulfide bonds and to support the idea of the impossibility of passage of the substrate in this mutant form. The quality of MD simulations was approved after the visual inspection of MD trajectories. The RMSD to the average structure obtained from the root mean square fluctuations (RMSF) analysis (Figure 4) decreases rapidly in the first MD simulation part, and from 5 ns stabilizes and oscillates around 1.0 Å (the main chain conformation is slightly more stable than side chains). The RMSD with respect to the crystal structure is increasing to the plateau value of 1.5 Å (non-hydrogen atoms) and 2.0 Å (for main chain atoms), indicating significant changes in the structure after introducing disulfide bond. Both these analyses suggest a generally stable structure of LinB D147C+L177C mutant during 50 ns MD simulation at 300K.

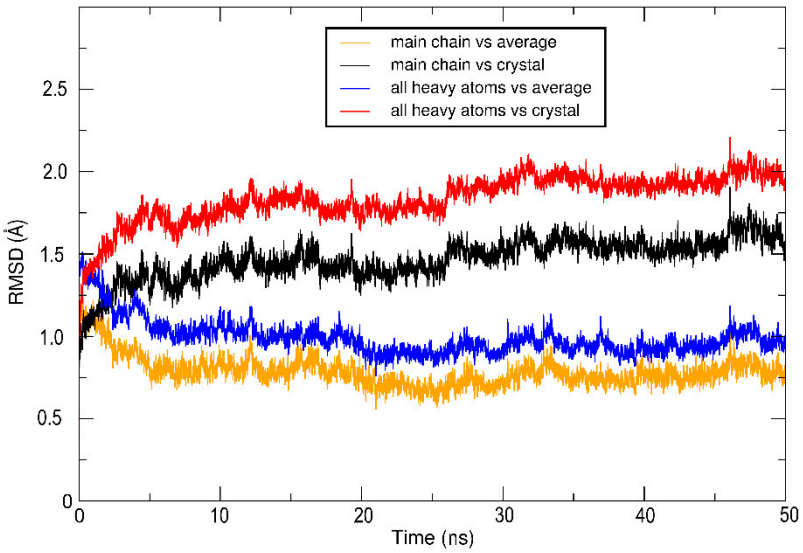

Figure 4. Molecular dynamics (MD) time series of root mean square deviation (RMSD) for LinB^{MD} D147C+L177C at 300 K. RMSD of the protein main chain with respect to the MD average structure is shown in orange; the protein main chain with respect to the crystal structure is in black; RMSD of non-hydrogen atoms with respect to the MD average structure is in blue, and RMSD of non-hydrogen atoms with respect to the crystal structure is in red.

To estimate the flexibility of the individual residues, the root mean square fluctuation (RMSF) analysis of each amino acid residue around its average position over the MD trajectory was performed. The resulting plot (Figure 5a) and the 3D model of LinB^{MD} D147C+L177C (Figure 5b) colored by RMSF values show highly flexible residues, especially close to regions of the disulfide bridge as well as the N– and C– terminal parts. RMSF value of the residues fluctuates from 0.3 to 2.2 Å in the entire simulation time; the most flexible part of the protein structure is close to Cys147 with RMSF of 2.0 Å.

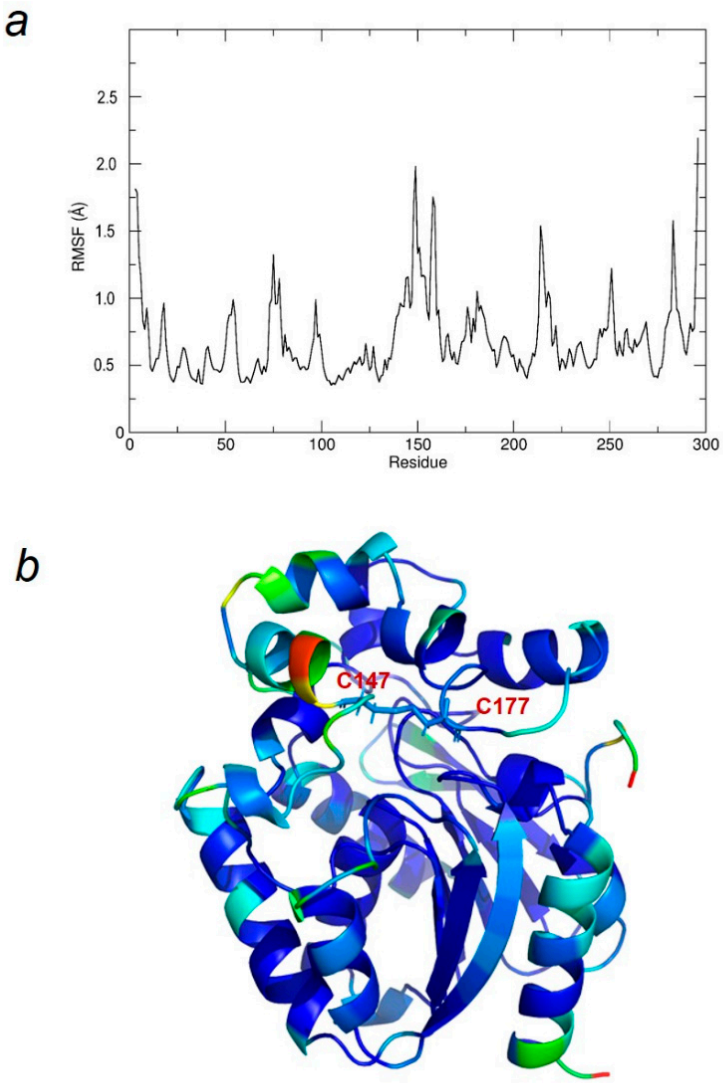

Figure 5. Flexibility of LinB^{MD} D147C+L177C individual residues. (**a**) The RMSF of LinB D147C+L177C mutant during MD simulation at 300 K; (**b**) LinB^{MD} D147C+L177C mutant represented as a 3D cartoon model with each residue coloured by RMSF values in the range from 0.03 nm (= 0.3 Å, blue) to 0.22 nm (= 2.2 Å, red), D147C-L177C disulfide bond shown as sticks.

The final analysis of MD simulations estimated the radius of gyration (Figure 6), which is defined as the mass-weighted root mean square distance of collection atoms from their common center of mass. The R_g value was oscillating around 17.6 to 17.9 Å, which indicates the stability of the protein tertiary structure during the whole simulation time.

The average molecular structure LinB^{MD} D147C+L177C was extracted from the MD trajectory and used in the following substrate docking study. The overall fold of LinB D147C+L177C crystal structure and LinB^{MD} D147C+L177C are similar, and the main differences are in the area of D147C-L177C disulfide bond (Figure 7a).

To explore the complementarity between the substrate 1,2-dibromoethane (DBE) and the enzyme's active site of LinB D147C+L177C mutant with or without disulfide bridge, the molecular docking study was performed on the X-ray crystal structure and LinB^{MD} D147C+L177C structure, respectively. The docking study found the most favorable binding modes of a given substrate within the binding pocket (enzyme active site) in both mentioned protein structures. In the case of LinB^{MD} D147C+L177C, the substrate with the most favorable binding mode (energy score −2.6 kcal.mol^{-1}) was located 6.2 Å apart from the nucleophilic oxygen OD1 Asp108 (Figure 7b) whereas in the case of crystal structure LinB D147C+L177C, the position of the most favorable binding mode (energy

score −3.0 kcal.mol^{-1}) was only 3.6 Å far from OD1 Asp108. The substrate shows a better fit for the active site of the mutant's crystal structure with the missing disulfide bridge, fulfilling the necessary conditions for the nucleophilic attack [28].

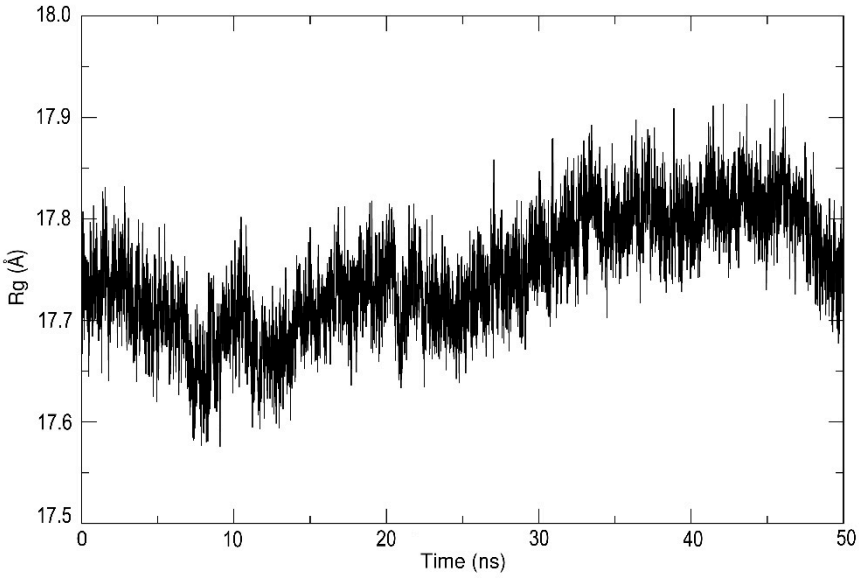

Figure 6. The radius of gyration (Rg) of the main chain atoms of LinB D147C+L177C during MD simulation at 300K.

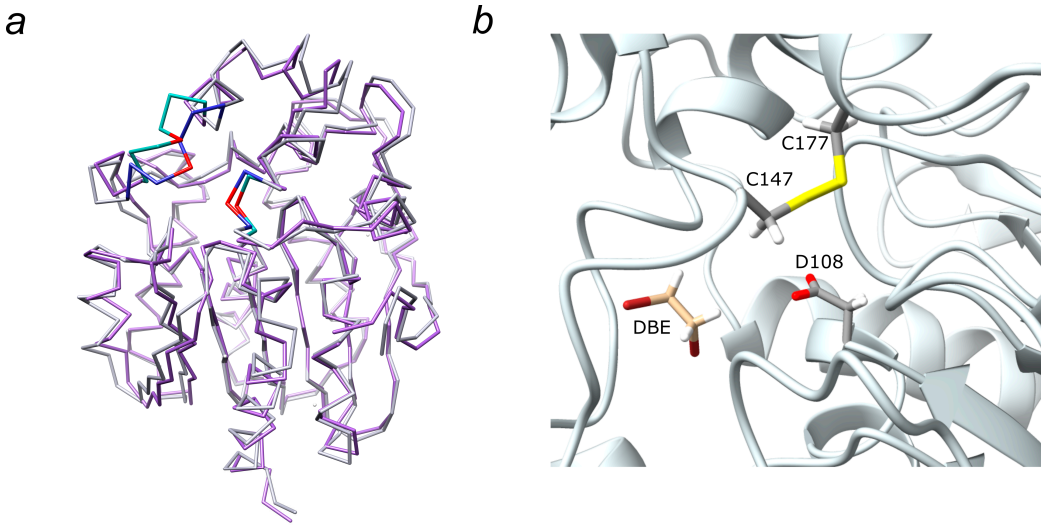

Figure 7. (**a**) Superposition of LinB D147C+L177C (purple) with LinB^{MD} D147C+L177C (grey). The residues 144–150 and 176–178 of LinB D147C+L177C are highlighted in turquoise, the residues 144–150 and 176–178 of LinB^{MD} D147C+L177C obtained from molecular dynamics simulations are in dark blue. Cys 147 and Cys 177 are in red. (**b**) 1,2-dibromethane (DBE) docked in the active site of LinB^{MD} D147C+L177C. Cysteine bridge C147–C177 and nucleophilic D108 are shown as sticks.

2.3. *Analysis of access Tunnels in LinB Variants*

The analysis of LinB WT (PDB ID: 2bfn, [18])) has shown two access tunnels (Figure 8a): the main tunnel (p1) consisting of upper (p1a) and lower (p1b) tunnels and a slot (p2), which is in accordance with previously reported data [5,29]. The lower tunnel has the widest bottleneck (1.6 Å) and thus plays a major role in the ligands and solvent transport [30].

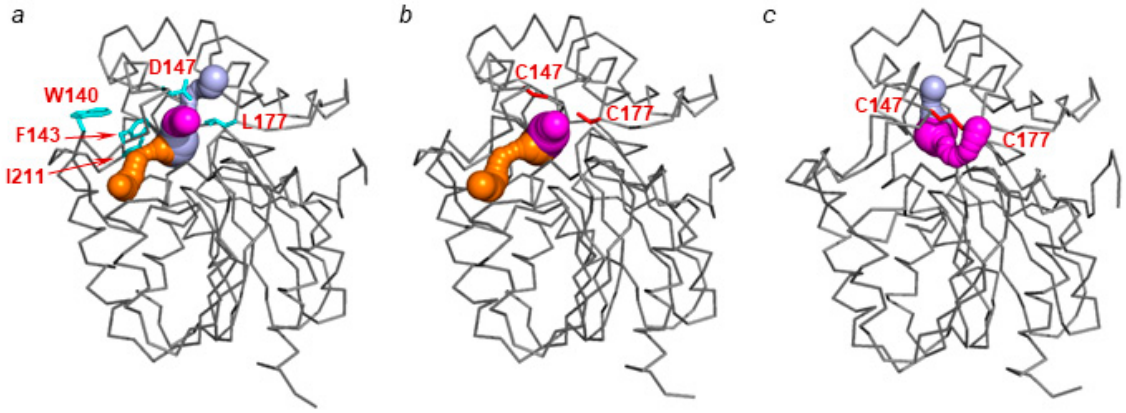

Figure 8. LinB access tunnels in (**a**) LinB WT (PDB ID: 2bfn, [18]), (**b**) LinB D147C+L177C crystal structure (PDB ID: 6s06, this study), and (**c**) LinB^{MD} D147C+L177C model. Tunnels p1a, p1b, and p2 are shown as light blue, magenta, and orange, respectively. The residues W140, F143, L177, and I211 are shown as blue sticks, while the substitutions D147C and L177C are shown as red sticks. The protein chain is shown as a grey ribbon.

In the crystal structure of LinB D147C+L177C, CAVER calculations [9,30] revealed the presence of two tunnels: p1b and p2. The width of both tunnels increased by 0.16 Å for p1b and by 0.1 Å for p2 tunnel compared with LinB WT (PDB ID: 2bfn, [18]). The p1a tunnel was not observed in the structure even with a smaller probe radius (Figure 8b). In the structure, C147 located in the mouth of the main tunnel is pulled away from C177 due to the crystal packing effect (Figure 3a). This causes the disruption of the disulfide bond between C147 and C177 and, therefore only partial closure of the main tunnel.

The calculated MD model of LinB^{MD} D147C+L177C contains a disulfide bridge between mutated cysteines (Figure 9a,b). The tunnels' analysis of the mutants unexpectedly revealed the presence of both p1a and p1b branches of the main tunnel, although with altered trajectory, and the closure of p2 tunnel (Figure 8c). The p1a tunnel was not detected in any of the studied LinB tunnel mutants previously. The p1b is 0.75 Å narrower, while the bottleneck of p1a is 0.16 Å wider compared with LinB WT (PDB ID: 2bfn, [18]) (Table 1). Additionally, the p1a is 5 Å shorter, making it comparable with p1b tunnel of LinB WT (PDB ID: 2bfn, [18]) (Table 1). The presence of alternative p1a and p1b tunnels in the mutant with the introduced disulfide bridge enables the accessibility to the enzyme's active site, which is in agreement with the previously identified residual activity of the mutant towards the best LinB WT substrate 1,2-dibromoethane [12].

Table 1. Geometry of the access tunnels calculated for different LinB variants using the software CAVER [31].

Structure		LinB WT	LinB D147C+L177C	LinB^{MD} D147C+L177C
PDB ID		2bfn	6s06	n/a
Bottleneck radius, Å	p1a	1.1	- [a]	1.2
	p1b	1.6	1.8	1.0
	p2	1.0	1.1	- [a]
Tunnel length, Å	p1a	13.4	- [a]	8.4
	p1b	8.6	6.7	17.5
	p2	13.8	15.0	- [a]

[a] Tunnel was not identified using the selected probe size.

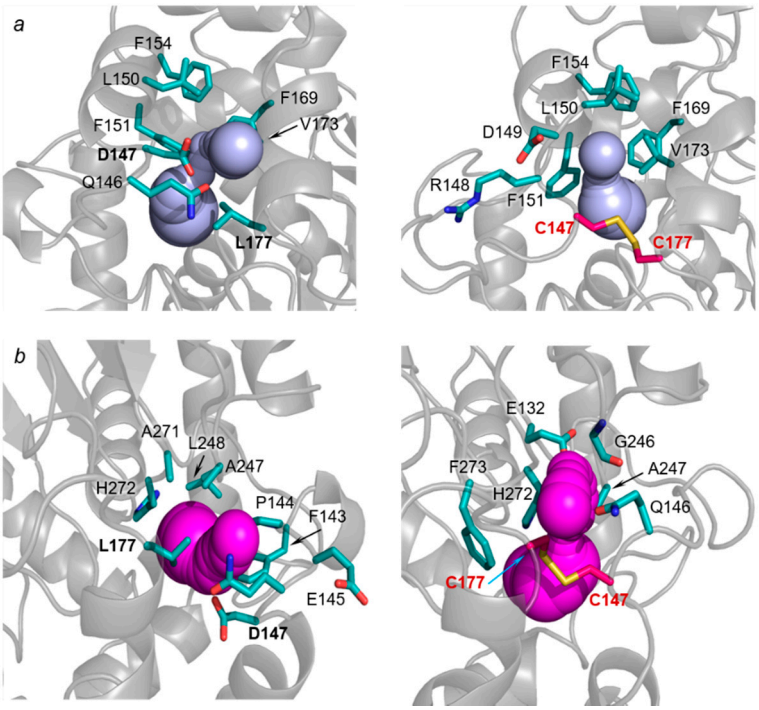

Figure 9. Close up view of (**a**) p1a and (**b**) p1b access tunnels in LinB WT (left, PDB ID: 2bfn, [18]) and LinB^{MD} D147C+L177C (right). The tunnels are shown as blue (p1a) and magenta (p1b) spheres, the sidechains of bottleneck residues are shown as cyan sticks, the disulfide bridge is shown as red-yellow sticks.

Protein tunnels play an important role in LinB function. Structural modifications of access tunnels provide enzymes with altered activity, specificity, stability, and even crystallization behavior [12,30]. The introduction of a cysteine bridge in LinB D147C+L177C with a goal to close the main access tunnel resulted in decreased activity for all of 30 different halogenated compounds tested [12]. This structural modification has introduced strain and flexibility in the structure of the enzyme and therefore restricted the crystallization of this mutant. Despite this fact, X-ray structure of LinB D147C+L177C was solved and its overall structure has shown high similarity to the structures of LinB WT (PDB ID: 2bfn, [18])) and LinB W140A+F143L+L177W+I211L [12]. Although the mutant was crystallized in conditions typical for various haloalkane dehalogenases, its crystallization took one and a half years, which is strikingly different from the days typically needed for crystallization of other LinB variants. Another encountered problem was the noisy signal for amino acids in the vicinity of introduced mutations, indicating the presence of several possible conformations of the region. MD simulations confirmed that even with the cysteine bridge formed, this part of the protein remains flexible. Analysis of the transport tunnels of LinB^{MD} D147C+L177C has unexpectedly shown alteration of both branches of the main tunnel and a closure of the auxiliary tunnel as a result of introduced disulfide bridge. Absence of the second tunnel hampered substrate and product passage between the active site and the surface, since substrates and products have to compete for the same tunnel in such a mutant. As a consequence, structurally and chemically different substrates—chlorinated, brominated, iodinated versus linear, and cyclic—hit the same rate-limiting step, product release, which resulted in highly similar activities [12]. The mutants with one of the access tunnels closed, LinB D147C+L177C and LinB L177W, confirm the importance of spatial separation of substrate and product fluxes for the efficiency of LinB enzyme.

3. Materials and Methods

3.1. Macromolecule Production

The mutant recombinant gene *linB D147C+L177C* was constructed by inverse PCR using Pfu DNA polymerase (Finnzymes, Espoo, Finland) with the following oligonucleotides: (forward: 5′-GGA TTT TCC CGA ACA GTG TCG CGA TCT GTT TC-3′ and reverse: 5′-GCC CAT TCG ATC GGC ATG GCG ATC GC-3′) as described previously [12]. The LinB variant had a C-terminal hexahistidyl tail enabling purification by metal-affinity chromatography. To overproduce the LinB D147C+L177C in *Escherichia coli*, the corresponding gene was subcloned into the expression vector pAQN under the control of the T7lac promoter (Novagen, Madison, WI, USA), and gene expression was induced by the addition of isopropyl-β-D-thiogalactoside (IPTG). *E. coli* BL21 cells containing the pAQN vector were cultured in 4 L of LB medium at 37 °C. When the culture reached an optical density of 0.5 at a wavelength of 600 nm, enzyme expression (at 20 °C) was induced by the addition of IPTG to a final concentration of 0.5 mM. The cells were harvested, disrupted by sonication using an Ultrasonic UP200S processor (Hielscher, Teltow, Germany), and centrifuged for 1 h at 4 °C and 21000g. The enzyme was purified on a Ni-NTA Superflow column (Qiagen, Hilden, Germany) attached to Äkta FPLC (GE Healthcare, Uppsala, Sweden) as described previously [12]. The purified protein was pooled and dialyzed against 50 mM Tris-HCl buffer (pH 7.5) overnight at 4 °C and stored in the same buffer at 4 °C until use.

3.2. Crystallization

Crystallization of LinB WT, LinB L177W, and LinB W140A+F143L+L177W+I211L was reported previously [5,12]. LinB wild type crystallization conditions, as well as conditions for LinB L177W and LinB W140A+F143L+L177W+I211L, were tried for LinB D147C+L177C, as there are only several point-mutation differences between them. However, the result was only heavy precipitation, and to find a suitable precipitant for LinB D147C+L177C the initial screening with the Gryphon crystallization robot (Art Robbins Instruments, Sunnyvale, CA, USA) was performed using various screens from Hampton Research Aliso Viejo, CA, (USA), Molecular Dimensions Ltd. (Sheffield, UK), and Qiagen (Venlo, The Netherlands). Both initial screening and optimization of crystallization conditions were carried out by sitting-drop vapor-diffusion technique in MRC 2-well crystallization plates (Hampton Research, Aliso Viejo, CA, USA) and 24-well CombiClover crystallization plates (Rigaku Reagents, Bainbridge Island, WA, USA), respectively. Optimization included a variation of temperature, pH, protein and precipitant concentrations and ratios.

3.3. Data collection and Processing, Structure Solution and Refinement

Data collection, processing, structure determination, and refinement for LinB WT, LinB L177W, and LinB W140A+F143L+L177W+I211L was described previously [5,12]. X-ray diffraction data for LinB D147C+L177C were collected at the BL14.1 beamline of the Joint Berlin MX Laboratory at the BESSY II electron storage ring in Berlin-Adlershof (Berlin, Germany) equipped with a PILATUS 6M detector (Dectris, Baden-Daettwil, Switzerland) at 100 K. Data collection was controlled by MxCuBE software system [31] and the strategy of data collection was determined with the help of iMosflm [32] to run Mosflm [33]. Cryoloops from Molecular Dimensions Ltd. (Sheffield, UK) and Hampton Research (Aliso Viejo, CA, USA) were used to mount crystals for the measurements. No additional cryoprotectant was applied before cooling the crystals in liquid nitrogen. The diffraction data set was processed with XDS [34] using XDSAPP graphical user interface [35] (data processing and refinement statistics in Table 2).

Table 2. Data processing, structure determination and refinement statistics of LinB D147C+L177C variant. Values in parentheses are for the highest resolution shell.

Diffraction source	BL14.1, BESSY II
Wavelength (Å)	0.9184
Temperature (K)	100
Detector	PILATUS 6M
Crystal-detector distance (mm)	210.545
Rotation range per image (°)	0.1
Total rotation range (°)	200
Exposure time per image (s)	0.5
Space group	$P2_12_12_1$
a, *b*, *c* (Å)	44.72, 68.71, 80.61
α, β, γ (°)	90.0 90.0 90.0
Mosaicity (°)	0.142
Resolution range (Å)	50.00–1.15 (1.22–1.15)
Total No. of reflections	550,609
No. of unique reflections	88,614
Completeness (%)	99.1 (98.4)
$CC_{1/2}$	99.9 (86.8)
$\langle I/\sigma(I)\rangle$	14.93 (2.60)
$R_{r.i.m.}$	6.9 (67.0)
Overall *B* factor from Wilson plot (Å^2)	18.18
Refinement program	*SHELXL*
No. of reflections, working set	84,016
No. of reflections, test set	4431
Final R_{cryst}	15.29
Final R_{free}	20.41
R.m.s. deviations	
Bonds (Å)	0.0128
Angles (°)	0.0205 [a]
Average B factors (Å2)	15.00
No. of protein atoms	2272
No. of chloride ions	1
No. of magnesium ions	3
No. of water molecules	233
Clashscore, all atom (%)	98
Ramachandran plot	
Most favoured (%)	97
Allowed (%)	3
PDB ID	**6s06**

[a] in SHELXL r.m.s. deviations in angles are calculated as deviations in the distances between atoms composing the angle.

The phase problem for the LinB D147C+L177C data set was solved by the molecular replacement method using the structure of wild-type LinB (PDB ID: 1cv2, [5]) as a search model. MOLREP program [36], a part of the CCP4 software package, was used for molecular replacement. LinB D147C+L177C structure was refined using SHELXL [37] for automated and Coot [38] for manual refinement. The model geometry (e.g., bond length, angles, Ramachandran plot, clashes) and agreement between the structure and experimental data were validated using Coot and the wwPDB Validation Server at http://wwpdb-validation.wwpdb.org/validservice/.

The structure of LinB D147C+L177C variant was deposited in the Protein Data Bank [39] under accession code 6s06.

3.4. Molecular Dynamics Simulations and Docking Studies

The initial molecular structure of LinB D147C+L177C mutant obtained from our crystallization experiments was modified by the formation of a disulfide bridge using Chimera 1.3.1 [23] and the whole structure was consecutively processed using the molecular dynamics software Gromacs 2016.3 [40,41] with OPLS-AA/L all-atom force field. The molecular system was solvated in a cubic water box using SPC/E 3-point water model. To neutralize the net charge on the protein the ions were included into the system. The initial steps of preparation the system for the production of MD simulations involved energy minimization by finding the local energy minimum, adjustment of the particular distribution of solvent molecules, and relaxation of possible steric clashes. Further, a short MD simulation was performed with harmonic position restraints on the heavy protein atoms with an integration step of 2fs. The solvent and ions around the protein were equilibrated in two phases, the first one under 0.01ns NVT (constant Number of particles, Volume, and Temperature) ensemble and the second under 0.01ns NPT (constant Number of particles, Pressure, and Temperature) ensemble. The velocity rescaling thermostat (improvement upon the Berendsen weak coupling method) and Parrinello-Rahman barostat were used for NVT equilibration and for pressure coupling in NPT phase, respectively. Electrostatic interactions were assessed by PME (Particle Mesh Ewald) method. Upon completion of both phases, the system was equilibrated at the preferred temperature 300K and pressure 1atm. Finally, production dynamics simulations were done with released position restraints; and 50ns molecular dynamics trajectories were calculated at a constant temperature of 300K and a pressure of 1atm. Following visual inspection of the molecular dynamics trajectory, some standard checks of the simulations quality have been performed by the analysis tools involved in Gromacs package.

The following properties have been investigated: root mean square deviation (RMSD) to the X-ray structure and to the average structure, root mean square fluctuation (RMSF) to reproduce the flexibility of protein residues (could be compared to crystallographic B-factors), and finally radius of gyration (Rg) as a measure of the molecular shape and compactions level at each time.

To explore the accessibility of substrate 1,2-dibromoethane to the enzyme's active site of LinB D147C+L177C mutant and LinB^{MD} D147C+L177C, the molecular docking study was performed by using AutoDock Vina v.1.1.2 [42] implemented in Chimera 1.3.1. The crystal structure of LinB D147C+L177C mutant and LinB^{MD} D147C+177C were docked with their substrate, 1,2-dibromoethane, which was obtained from the Pubchem database [43] and its molecular geometry was optimized using Chimera [23]. Hydrogens and charges were added to the ligand and receptor. The docking searches were performed with exhaustiveness of 8, 10 modes and energy range of 3kcal.mol^{-1}. Searches were carried out over the whole molecule allowing the ligands to be flexible. The ViewDock tool in Chimera package was used to facilitate interactive analysis of receptor-ligand docking results. Different poses of a ligand were viewed individually in the context of a binding site and were ranked by energy score, which follows X-Score [42] scoring function for binding free energy for protein-ligand complexes with known 3D structures. The involvement of active site residues in the substrate binding was examined by DS Visualizer ver. 20.1.0.19295 [42], which provided all types of non-covalent interactions in the 2D diagram.

3.5. Analysis of Access Tunnel

The analysis of the access tunnels was performed by Caver 3.0 PyMOL Plugin [33,34] as described previously [5]. Briefly, the coordinates of the crystal structure of LinB WT (PDB ID: 2bfn, [18]) was downloaded from the RCSB PDB database [43]. The crystal structure of LinB D147C+L177C (PDB ID 6s06, this study) and MD model LinB^{MD} D147C+L177C were newly obtained, respectively. The solvent molecules, ligands, alternative conformations of amino acids, and hydrogens in MD model were removed from the structures prior to tunnel calculations. The structures were superimposed on LinB WT (PDB ID: 2bfn, [18]) using PyMOL 1.7, and the starting point was set in the position 15.977, 14.744, 22.053 Å.

Transport tunnels were identified using a probe radius of 1.0 Å, and tunnels were clustered using the threshold of 3.5.

4. Conclusions

Our structural and modeling studies show that the introduction of the disulfide bridge has, surprisingly, enhanced the flexibility of regions around the disulfide bridge, which resulted in difficulties to crystallize the mutant. The tunnel analysis of LinB^{MD} D147C+L177C has shown the closure of the secondary tunnel and alteration of the main tunnel as a result of disulfide bridge presence. These changes affect the accessibility of the substrate to the catalytic site, hamper product release and decrease catalytic activity of LinB D147C+L177C mutant for a wide variety of substrates.

Author Contributions: Conceptualization, I.K.S. and J.D.; methodology, R.C.; software, I.I., O.D. and M.K.; validation, I.I., O.D., T.P. and M.K.; formal analysis, I.I., O.D. and T.P.; investigation and resources, I.K.S. and J.D.; data curation, P.H.; writing—original draft preparation, I.I., O.D. and P.H.; writing—review and editing, I.I., O.D., T.P., I.K.S. and R.C.; visualization, I.I., O.D., M.K. and T.P.; supervision, I.K.S. and J.D.; project administration and funding acquisition, I.K.S. All authors have read and agreed to the published version of the manuscript.

Funding: This work was supported by ERDF project CZ.02.1.01/0.0/0.0/15_003/0000441, GAJU 17/2019/P and Czech Ministry of Education CZ.02.1.01/0.0/0.0/16_026/0008451, LM2018121 and LM2015047, and previous Czech Science Foundation grant GACR (17-24321S).

Institutional Review Board Statement: Not applicable.

Informed Consent Statement: Not applicable.

Acknowledgments: We thank Jeroen R. Mesters for helping with data processing and structure refinement.

Conflicts of Interest: No interest conflict exists among the authors.

References

1. Janssen, D.B.; Dinkla, I.J.T.; Poelarends, G.J.; Terpstra, P. Bacterial degradation of xenobiotic compounds: Evolution and distribution of novel enzyme activities: Evolution and distribution of novel enzyme activities. *Environ. Microbiol.* **2005**, *7*, 1868–1882. [CrossRef]
2. Hynkova, K.; Nagata, Y.; Takagi, M.; Damborsky, J. Identification of the catalytic triad in the haloalkane dehalogenase from Sphingomonas paucimobilis UT26. *FEBS Lett.* **1999**, *446*, 14747–14753. [CrossRef]
3. Nagata, Y.; Miyauchi, K.; Damborsky, J.; Manova, K.; Ansorgova, A.; Takagi, M. Degradation of β-Hexachlorocyclohexane by Haloalkane Dehalogenase LinB from Sphingomonas paucimobilis UT26. *Appl. Environ. Microbiol.* **1997**, *63*, 3707–3710. [CrossRef]
4. Prokop, Z.; Monincova, M.; Chaloupkova, R.; Klvana, M.; Nagata, Y.; Janssen, D.B.; Damborsky, J. Structure–Function Relationships and Engineering of Haloalkane Dehalogenases. *J. Biol. Chem.* **2003**, *278*, 45094–45100. [CrossRef] [PubMed]
5. Marek, J.; Vevodova, J.; Kuta Smatanova, I.; Nagata, Y.; Svensson, L.A.; Newman, J.; Takagi, M.; Damborsky, J. Protein engineering of haloalkane dehalogenase LinB: Reconstruction of active site and modification of entrance tunnel. *Biochemistry* **2000**, *39*, 177–181.
6. Chovancova, E.; Kosinski, J.; Bujnicki, M.J.; Damborsky, J. Phylogenetic Analysis of Haloalkane Dehalogenases. *Proteins* **2007**, *67*, 305–316. [CrossRef] [PubMed]
7. Bohac, M.; Nagata, Y.; Prokop, Z.; Prokop, M.; Monincova, M.; Koca, J.; Tsuda, M.; Damborsky, J. Halide-stabilizing residues of haloalkane dehalogenases studied by quantum mechanic calculations and site-directed mutagenesis. *Biochemistry* **2002**, *41*, 14272–14280. [CrossRef] [PubMed]
8. Nagata, Y.; Nariya, T.; Ohtomo, R.; Fukuda, M.; Yano, K.; Takagi, M. Cloning and sequencing of a dehalogenase gene encoding an enzyme with hydrolase activity involved in the degradation of gamma-hexachlorocyclohexane in Pseudomonas paucimobilis. *J. Bacteriol.* **1993**, *175*, 6403–6410. [CrossRef]
9. Chovancova, E.; Pavelka, A.; Benes, P.; Strnad, O.; Brezovsky, J.; Kozlikova, B.; Gora, A.; Sustr, V.; Klvana, M.; Medek, P.; et al. CAVER 3.0: A Tool for the Analysis of Transport Pathways in Dynamic Protein Structures. *PLoS Comput. Biol.* **2012**, *8*, e1002708. [CrossRef]
10. Biedermannova, L.; Prokop, Z.; Gora, A.; Chovancova, E.; Kovacs, M.; Damborsky, J.; Wade, R.C. A Single Mutation in a Tunnel to the Active Site Changes the Mechanism and Kinetics of Product Release in Haloalkane Dehalogenase LinB. *J. Biol. Chem.* **2012**, *287*, 29062–29074. [CrossRef]
11. Oakley, A.J.; Klvana, M.; Otyepka, M.; Nagata, Y.; Wilce, M.C.; Damborsky, J. Crystal structure of haloalkane dehalogenase LinB from Sphingomonas paucimobilis UT26 at 0.95 A resolution: Dynamics of catalytic residues. *Biochemistry* **2004**, *43*, 870–878. [CrossRef] [PubMed]

12. Brezovsky, J.; Babkova, P.; Degtjarik, O.; Fortova, A.; Gora, A.; Iermak, I.; Rezacova, P.; Dvorak, P.; Kuta Smatanova, I.; Prokop, Z.; et al. Engineering a de Novo Transport Tunnel. *ACS Catal.* **2016**, *6*, 7597–7610. [CrossRef]
13. Pavlova, M.; Klvana, M.; Prokop, Z.; Chaloupkova, R.; Banas, P.; Otyepka, M.; Wade, R.C.; Tsuda, M.; Nagata, Y.; Damborsky, J. Redesigning dehalogenase access tunnels as a strategy for degrading an anthropogenic substrate. *Nat. Chem. Biol.* **2009**, *5*, 727–733. [CrossRef] [PubMed]
14. Prokop, Z.; Gora, A.; Brezovsky, J.; Chaloupkova, R.; Stepankova, V.; Damborsky, J. Engineering of protein tunnels: Keyhole-lock-key model for catalysis by the enzymes with buried active sites. *Prot. Eng. Handb.* **2012**, *3*, 421–464.
15. Zhou, G.; Somasundaram, T.; Blanc, E.; Parthasarathy, G.; Ellington, W.R.; Chapman, M.S. Transition state structure of arginine kinase: Implications for catalysis of bimolecular reactions. *Proc. Natl. Acad. Sci. USA* **1998**, *95*, 8449–8454. [CrossRef]
16. Liebgott, P.-P.; Leroux, F.; Burlat, B.; Dementin, S.; Baffert, C.; Lautier, T.; Fourmond, V.; Ceccaldi, P.; Cavazza, C.; Meynial-Salles, I.; et al. Relating diffusion along the substrate tunnel and oxygen sensitivity in hydrogenase. *Nat. Chem. Biol.* **2010**, *6*, 63–70. [CrossRef]
17. Chaloupkova, R.; Sykorova, J.; Prokop, Z.; Jesenska, A.; Monincova, M.; Pavlova, M.; Tsuda, M.; Nagata, Y.; Damborsky, J. Modification of activity and specificity of haloalkane dehalogenase from Sphingomonas paucimobilis UT26 by engineering of its entrance tunnel. *J. Biol. Chem.* **2003**, *278*, 52622–52628. [CrossRef]
18. Minincova, M.; Prokop, Z.; Vevodova, J.; Nagata, Y.; Damborsky, J. Weak Activity of Haloalkane Dehalogenase Linb with 1,2,3-Trichloropropane Revealed by X-Ray Crystallography and Microcalorimetry. *Appl. Environ. Microbiol.* **2007**, *73*, 2005–2008. [CrossRef] [PubMed]
19. Eldar, A.; Rozenberg, H.; Diskin-Posner, Y.; Rohs, R.; Shakked, Z. Structural studies of p53 inactivation by DNA-contact mutations and its rescue by suppressor mutations via alternative protein-DNA interactions. *Nucleic Acids Res.* **2013**, *41*, 8748–8759. [CrossRef]
20. Okai, M.; Ohtsuka, J.; Imai, L.F.; Mase, T.; Moriuchi, R.; Tsuda, M.; Nagata, K.; Nagata, Y.; Tanokura, M. Crystal structure and site-directed mutagenesis analyses of haloalkane dehalogenase linB from sphingobium sp. Strain MI1205. *J. Bacteriol.* **2013**, *195*, 2642–2651. [CrossRef]
21. Prudnikova, T.; Mozga, T.; Rezacova, P.; Chaloupkova, R.; Sato, Y.; Nagata, Y.; Brynda, J.; Kuty, M.; Damborsky, J.; Kuta Smatanova, I. Crystallization and Preliminary X-ray Analysis of a Novel Haloalkane Dehalogenase DbeA from Bradyrhizobium elkani USDA94. *Acta Crystallogr. Sect. F Struct. Biol. Cryst. Commun.* **2009**, *65*, 353–356. [CrossRef] [PubMed]
22. Degtjarik, O.; Chaloupkova, R.; Rezacova, P.; Kuty, M.; Damborsky, J.; Kuta Smatanova, I. Differences in crystallization of two LinB variants from Sphingobium japonicum UT26. *Acta Crystallogr. Sect. F Struct. Biol. Cryst. Commun.* **2013**, *69*, 284–287. [CrossRef] [PubMed]
23. Pettersen, E.F.; Goddard, T.D.; Huang, C.C.; Couch, G.S.; Greenblatt, D.M.; Meng, E.C.; Ferrin, T.E. UCSF Chimera—A visualization system for exploratory research and analysis. *J. Comput. Chem.* **2004**, *13*, 1605–1612. [CrossRef]
24. DeLano, W.L. PyMol. The PyMOL Molecular Graphics System, Version 2.0 Schrödinger, LLC. 2002. Available online: http://www.pymol.org (accessed on 14 September 2020).
25. Streltsov, V.A.; Prokop, Z.; Damborsky, J.; Nagata, Y.; Oakley, A.; Wilce, M.C.J. Haloalkane dehalogenase LinB from Sphingomonas paucimobilis UT26: X-ray crystallographic studies of dehalogenation of brominated substrates. *Biochemistry* **2003**, *42*, 10104–10112. [CrossRef] [PubMed]
26. Krissinel, E.; Henrick, K. Detection of Protein Assemblies in Crystals. *Acta Crystallogr. Sect. D Biol. Crystallogr.* **2004**, *60*, 2256–2268. [CrossRef] [PubMed]
27. Winn, M.D.; Ballard, C.C.; Cowtan, K.D.; Dodson, E.J.; Emsley, P.; Evans, P.R.; Keegan, R.M.; Krissinel, E.B.; Leslie, A.G.W.; McCoy, A.; et al. Overview of the CCP4 suite and current developments. *Acta Crystallogr. Sect. D Biol. Crystallogr.* **2011**, *67*, 235–242. [CrossRef]
28. Negri, A.; Marco, E.; Damborsky, J.; Gago, F. Stepwise Dissection and Visualization of the Catalytic Mechanism of Haloalkane Dehalogenase LinB using Molecular Dynamics Simulations and Computer Graphics. *J. Mol. Graph. Model.* **2007**, *26*, 643–651. [CrossRef]
29. Kokkonen, P.; Bednar, D.; Pinto, G.; Prokop, Z.; Damborsky, J. Engineering Enzyme Access Tunnels. *Biotechnol. Adv.* **2019**, *37*, 107386. [CrossRef]
30. Petrek, M.; Otyepka, M.; Banas, P.; Kosinova, P.; Koca, J.; Damborsky, J. CAVER: A New Tool to Explore Routes from Protein Clefts, Pockets and Cavities. *BMC Bioinform.* **2006**, *7*, 316. [CrossRef]
31. Gabaldinho, J.; Beteva, A.; Guijarro, M.; Rey-Bakaikoa, S.D.; Bowler, M.W.; Brockhauser, S.; Flot, D.; Gordon, D.F.; Hall, D.R.; Lavault, B.; et al. MxCuBE: A synchrotron beamline control environment customized for macromolecular crystallography experiments. *J. Synchrotron Radiat.* **2010**, *17*, 700–707. [CrossRef]
32. Battye, T.G.G.; Kontogiannis, L.; Jonson, O.; Powell, H.R.; Leslie, A.G.W. iMOSFLM: A new graphical interface for diffraction-image processing with MOSFLM. *Acta Crystallogr. Sect. D Biol. Crystallogr.* **2011**, *67*, 271–281. [CrossRef] [PubMed]
33. Leslie, A.G. The integration of macromolecular diffraction data. *Acta Crystallogr. Sect. D Biol. Crystallogr.* **2006**, *62*, 48–57. [CrossRef] [PubMed]
34. Kabsch, W. XDS. *Acta Crystallogr. Sect. D Biol. Crystallogr.* **2010**, *66*, 125–132. [CrossRef] [PubMed]
35. Krug, M.; Weiss, M.S.; Heinemann, U.; Mueller, U. XDSAPP2.0. *J. Appl. Crystallogr.* **2010**, *45*, 568–572. [CrossRef]
36. Vagin, A.; Teplyakov, A. MOLREP: An Automated Program for Molecular Replacement. *J. Appl. Crystallogr.* **1997**, *30*, 1022–1025. [CrossRef]

37. Sheldrick, G.M.; Schneider, T.R. SHELXL: High-resolution refinement. *Meth. Enzymol.* **1997**, *277*, 319–343.
38. Emsley, P.; Lohkamp, B.; Scott, W.G.; Cowtan, K. Features and development of Coot. *Acta Crystallogr. Sect. D Biol. Crystallogr.* **2010**, *66*, 486–501. [CrossRef]
39. Berman, H.M.; Westbrook, J.; Feng, Z.; Gilliland, G.; Bhat, T.N.; Weissig, H.; Shindyalov, I.N.; Bourne, P.E. The Protein Data Bank. *Nucleic Acids Res.* **2000**, *28*, 235–242. [CrossRef]
40. Berendsen, H.J.C.; van der Spoel, D.; van Drunen, R. GROMACS: A message-passing parallel molecular dynamics implementation. *Comput. Phys. Commun.* **1995**, *91*, 43–56. [CrossRef]
41. Lindahl, E.; Hess, B.; van der Spoel, D. GROMACS 3.0: A package for molecular simulation and trajectory analysis. *Mol. Model. Annu.* **2001**, *7*, 306–317. [CrossRef]
42. Trott, O.; Olson, J.A. AutoDock Vina: Improving the speed and accuracy of docking with a new scoring function, efficient optimization and multithreading. *J. Comput. Chem.* **2010**, *31*, 455–461. [CrossRef] [PubMed]
43. Kim, S.; Thiessen, P.A.; Bolton, E.E.; Chen, J.; Fu, G.; Gindulyte, A.; Han, L.; He, J.; He, S.; Shoemaker, B.A.; et al. PubChem Substance and Compound databases. *Nucleic Acids Res.* **2016**, *44*, 1202–1213. [CrossRef] [PubMed]